processes

Article

Feasibility of Advanced CO_2 Injection and Well Pattern Adjustment to Improve Oil Recovery and CO_2 Storage in Tight-Oil Reservoirs

Lijun Zhang [1,2], Tianwei Sun [1,2], Xiaobing Han [3], Jianchao Shi [4], Jiusong Zhang [3], Huiting Tang [3] and Haiyang Yu [3,*]

1 National Key Laboratory for Efficient Development of Offshore Oil, Beijing 100029, China
2 CNOOC Research Institute Company Limited, Beijing 100028, China
3 State Key Laboratory of Petroleum Resources and Prospecting, China University of Petroleum, Beijing 102249, China
4 Research Institute of Exploration and Development, PetroChina Changqing Oilfield Company, Xi'an 710018, China
* Correspondence: haiyangyu.cup@139.com

Abstract: Global tight-oil reserves are abundant, but the depletion development of numerous tight-oil reservoirs remains unsatisfactory. CO_2 injection development represents a significant method of reservoir production, potentially facilitating enhanced oil recovery (EOR) alongside CO_2 storage. Currently, limited research exists on advanced CO_2 injection and well pattern adjustment aimed at improving the oil recovery and CO_2 storage within tight-oil reservoirs. This paper focuses on the examination of tight oil within the Ordos Basin. Through the employment of slim-tube experiments, long-core displacement experiments, and reservoir numerical simulations, the near-miscible pressure range and minimum miscible pressure (MMP) for the target block were ascertained. The viability of EOR and CO_2 sequestration via advanced CO_2 injection was elucidated, establishing well pattern adjustment methodologies to ameliorate CO_2 storage and enhance oil recovery. Simultaneously, the impacts of the injection volume and bottom-hole pressure on the development of advanced CO_2 injection were explored in further detail. The experimental results indicate that the near-miscible pressure range of the CO_2–crude oil in the study area is from 15.33 to 18.47 MPa, with an MMP of 18.47 MPa, achievable under reservoir pressure conditions. Compared to continuous CO_2 injection, advanced CO_2 injection can more effectively facilitate EOR and achieve CO_2 sequestration, with the recovery and CO_2 sequestration rates increasing by 4.83% and 2.29%, respectively. Through numerical simulation, the optimal injection volume for advanced CO_2 injection was determined to be 0.04 PV, and the most favorable bottom-hole flowing pressure was identified as 10 MPa. By transitioning from a square well pattern to either a five-point well pattern or a row well pattern, the CO_2 storage ratio significantly improved, and the gas–oil ratio of the production wells also decreased. Well pattern adjustment effectively supplements the formation energy, extends the stable production lives of production wells, and increases both the sweep efficiency and oil recovery. This study provides theoretical support and serves as a reference for CO_2 injection development in tight-oil reservoirs.

Keywords: advanced CO_2 injection; well pattern adjustment; enhanced oil recovery; CO_2 storage; tight oil

check for updates

Citation: Zhang, L.; Sun, T.; Han, X.; Shi, J.; Zhang, J.; Tang, H.; Yu, H. Feasibility of Advanced CO_2 Injection and Well Pattern Adjustment to Improve Oil Recovery and CO_2 Storage in Tight-Oil Reservoirs. *Processes* **2023**, *11*, 3104. https://doi.org/10.3390/pr11113104

Academic Editors: Albert Ratner and Vladimir S. Arutyunov

Received: 3 October 2023
Revised: 20 October 2023
Accepted: 27 October 2023
Published: 29 October 2023

1. Introduction

Global tight-oil reserves are abundant [1,2], but numerous tight reservoirs still face the difficulty of efficient development, which is characterized by rapid production decline and low oil recovery [3,4]. CO_2 injection development is an important method of reservoir development, and the main mechanism is to supplement the formation energy [5–8], volume expansion [9–11], interfacial tension reduction [12,13], and viscosity reduction of the crude oil caused by the oil–gas interaction [14,15]. During CO_2 flooding development, injected gas can form the miscible phase with crude oil (exceeding the miscible pressure), reduce the interfacial tension between the oil and gas, and improve the oil displacement efficiency [16–19]. However, CO_2 flooding is greatly affected by reservoir heterogeneity and viscous fingering, leading to gas channeling in fractures or high-permeability channels, which make it difficult to maintain the formation pressure [20–24]. There are limited oilfield pilot projects concerning CO_2 injection development in tight reservoirs, and the methods for enhancing oil recovery, alongside efficient development strategies, necessitate further investigation.

Numerous scholars have conducted extensive research on CO_2 injection development in tight reservoirs, verifying the feasibility of such development through experiments and confirming the potential of CO_2 injection for EOR [25–27]. The numerical simulation method is used to conduct reservoir simulation research, and the impact laws of the key parameters are analyzed, including the injection pressure, gas injection rate, well-spacing, bottom-hole-pressure, and fracture parameters [28–30]. Through core displacement experiments, Fatemeh Kamali et al. [31] demonstrated that CO_2 flooding can EOR, and that the near-miscible displacement is close to the miscible displacement in oil recovery, which is about 18% higher than the immiscible displacement. Sheng and Chen [32] conducted reservoir simulation work on post-depletion gas flooding development, post-depletion gas injection huff-n-puff, and direct gas flooding through numerical simulation. The results indicate that the oil recovery factor of gas injection development is higher after depletion development.

As a promising technology, CO_2 injection development has the significant potential to enhance the production capabilities of oil reservoirs [33]. At present, CO_2 injection development has been widely used in conventional reservoirs (medium/high permeability, low permeability) [34]. In the Permian Basin of the United States, characterized by a permeability of 4.9 mD, the inverse five-point well pattern was chosen for the oilfield well arrangement, employing the vertical well type with a well spacing of 160 m. Additionally, all wells undergo acid-fracturing treatment. After production testing, CO_2 flooding had a significant effect on increasing the oil production, with a stable production of 3000 barrels/day, which can effectively exploit the remaining oil [35–37]. For the Monell Oilfield (20 mD) in the United States, the current block production is about 5500 barrels/month after nearly 20 years of gas injection development. Field test results demonstrate that the average oil recovery utilizing the inverse nine-point well pattern increases by 12~13% compared to that of the inverse five-point well pattern, thereby exhibiting an enhanced development performance. For the gas flooding of tight-oil reservoirs, the CO_2 injection pilot was conducted for the Bakken Oilfield (0.13 mD) in Canada [38–40]. The pilot block is dominated by fracturing horizontal-well development, with horizontal wells as the injection wells and vertical wells as the production wells, forming an approximate inverse five-point well pattern with a well spacing of 300 m. After the trial production, CO_2 flooding achieved good results. For gas injection development in low-permeability reservoirs, it is crucial to reasonably arrange the well patterns based on the fracture strike. The Qiaojiawa Oilfield, located in China (with an average permeability of 0.75 mD), has also conducted a CO_2 flooding pilot, with a total of 5 injection wells and 18 production wells, manifesting a good CO_2 injection performance. From the oilfield flooding effect, the cumulative oil increase is 1806.2 t.

Although CO_2 flooding can achieve good development results, the development of tight reservoirs is still faced with the problems of insufficient natural energy and the rapid decline of oil well production [41,42]. Therefore, advanced CO_2 injection is proposed to solve this problem and further improve the oil recovery of CO_2 flooding. Advanced CO_2 injection means that, before the production well is put into production, the injection well injects CO_2 in advance to increase the pressure of the formation, so that the formation pressure is higher than the original formation pressure, so as to establish a more effective displacement system [43,44]. Currently, there are few studies on advanced CO_2 injection development for tight reservoirs. Formulating reasonable advanced-injection strategies has great potential for enhancing oil recovery in tight-oil reservoirs [45]. CO_2 injection development can not only effectively enhance oil recovery, but it can also store plentiful greenhouse gases (e.g., CO_2) for geological storage, which has attracted extensive attention from global scholars [46–48]. The combination of CO_2-EOR and CO_2 storage targets the maximization of oil production and CO_2 storage [49].

Given the absence of advanced CO_2 injection pilot projects for tight-oil reservoirs, this study, through the execution of slim-tube and long-core displacement experiments, along with reservoir numerical simulations, verifies the feasibility of advanced CO_2 injection for tight-oil reservoirs. It evaluates the potential increase in the oil production and CO_2 storage efficacy afforded by advanced CO_2 injection, and it establishes well pattern adjustment methodologies to facilitate EOR and CO_2 storage. This study provides theoretical support and serves as a reference for the development of CO_2 injection strategies in tight reservoirs.

2. Experiments and Simulation

2.1. Experiments

2.1.1. Materials

Reservoir Cores

Measurement was conducted using a vernier caliper, revealing that the lengths of the core samples utilized in this study were approximately 7 cm, with diameters of around 2.5 cm. The core samples were obtained from the M block of the Changqing Oilfield at a depth of approximately 2650 m. The porosity and permeability of the core samples were determined using the TCLTS-1 porosity tester and the PDP-200 permeability tester, respectively. The porosity was determined via the helium porosity meter method, while the permeability was assessed utilizing the pulse decay method. The test results revealed a porosity ranging from 5.79% to 9.06% and a permeability ranging from 0.21 to 0.522 mD. Specific parameters of the experimental rock cores are provided in Table 1. Core1–Core8 were employed for conducting continuous gas injection experiments, while Core9–Core16 were designated for advanced gas injection experiments.

Table 1. Physical parameters of cores from target blocks.

Core	Diameter (cm)	Length (cm)	Porosity (%)	Permeability (mD)	Experiment
1	2.528	7.974	5.79	0.37	Continuous CO_2 injection
2	2.524	7.983	5.95	0.21	
3	2.524	7.966	6.35	0.27	
4	2.523	7.924	7.9	0.33	
5	2.525	7.959	8.04	0.23	
6	2.531	7.973	8.07	0.34	
7	2.528	7.971	7.43	0.48	
8	2.521	7.939	6.84	0.3	
9	2.521	7.956	7.06	0.3	Advanced CO_2 injection
10	2.531	7.955	6.76	0.21	
11	2.521	7.966	7.92	0.36	
12	2.526	7.969	8.26	0.33	
13	2.521	7.955	7.64	0.24	
14	2.531	7.954	9.06	0.34	
15	2.523	7.981	8.49	0.32	
16	2.524	7.993	8.56	0.522	

Formation Oil

The saturation pressure of the formation oil is 10.27 MPa, the oil density is about 733 kg/m^3, the oil viscosity is 1.21 mPa·s, and the dissolved gas–oil ratio is 85.34 m^3/m^3, which classifies it as low-viscosity light oil. Utilizing the surface degassed crude oil and associated gas obtained from Block M, the formation crude oil was formulated in accordance with the gas–oil ratio. Chromatography was utilized for the determination of the crude-oil constituents, relying on the principle that each component exhibits varying distribution coefficients between the mobile and stationary phases within the chromatographic column. The specific composition of this formulation is outlined in Table 2.

Table 2. Composition of crude oil.

Component	Mole Fraction (%)	Component	Mole Fraction (%)
CO_2	0.051	$C_{14\ H30}$	2.455
N_2	0.952	$C_{15\ H32}$	2.764
CH4	20.959	$C_{16\ H34}$	2.214
C_{2H6}	7.283	$C_{17\ H36}$	2.148
C_{3H8}	11.595	$C_{18\ H38}$	1.955
iC_{4H10}	2.774	$C_{19\ H40}$	1.892
nC_{4H10}	4.889	$C_{20\ H42}$	1.811
iC_{5H12}	2.256	$C_{21\ H44}$	1.724
nC_{5H12}	2.211	$C_{22\ H46}$	1.431
C_{6H14}	3.096	$C_{23\ H48}$	1.346
C_{7H16}	2.987	$C_{24\ H50}$	1.037
C_{8H18}	2.599	$C_{25\ H52}$	0.985
C_{9H20}	2.659	$C_{26\ H54}$	0.797
C_{10H22}	2.598	$C_{27\ H56}$	0.743
C_{11H24}	2.643	$C_{28\ H58}$	0.548
$C_{12\ H26}$	2.658	$C_{29\ H60}$	0.498
$C_{13\ H28}$	2.609	C_{30+}	0.837

Formation Brine

The composition and properties of the oilfield formation brine are shown in Table 3, with a total salinity of 35,420 mg L^{-1}, a brine type of $CaCl_2$, and a pH value of 6.62, showing weak acidity. The simulated formation briner was prepared according to the ion content in Table 3 for the subsequent experimental study.

Table 3. Formation water composition and properties.

Cationic (mg·L^{-1})			Anionic (mg·L^{-1})			Mineralization (mg·L^{-1})	Hydrated	PH
$K^+ + Na^+$	Ca^{2+}	Mg^{2+}	Cl^-	SO_4^{2-}	HCO_3^-			
6619	4742	325	22,919	716	186	35.4235,420	$CaCl_2$	6.62

2.1.2. Experimental Setup

Slim Tube

The miscible state of the CO_2–crude-oil mixture significantly affects the effectiveness of the CO_2 flooding. Consequently, slim-tube experiments were conducted to determine the minimum miscibility pressure and the near-miscibility pressure range, in order to determine whether the CO_2 flooding in the target reservoir is in a miscible or near-miscible phase. As illustrated in Figure 1, the fine-tube experimental system comprises an ISCO pump, an intermediate container, fine tubes, a back-pressure valve, a return pump, and a flow meter, among other components. By evaluating the displacement efficiency at varying pressures, both the minimum miscibility pressure and the near-miscibility pressure range are ascertained.

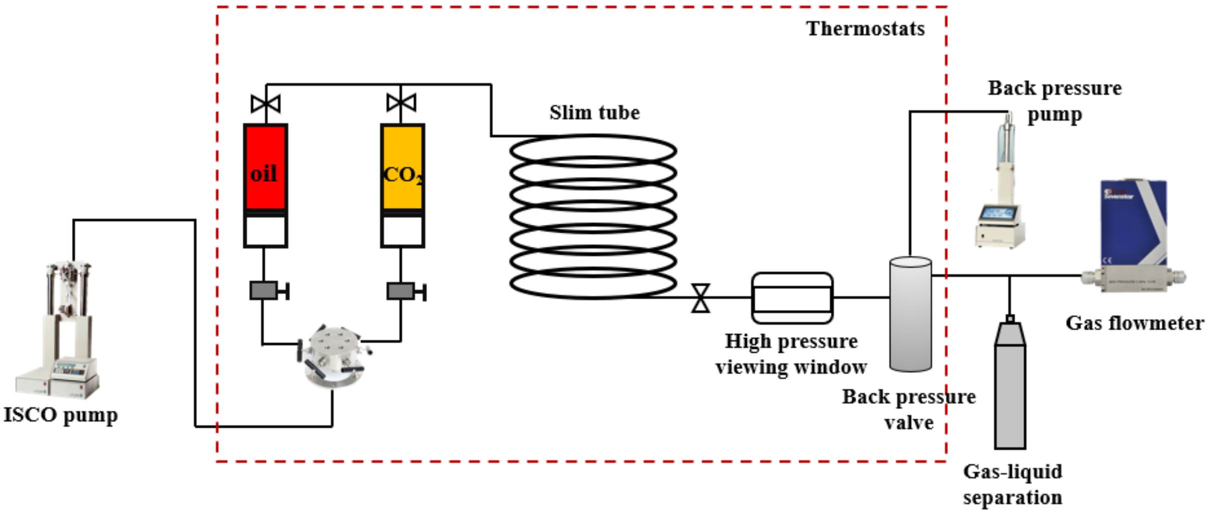

Figure 1. Schematic diagram of the slim-tube experimental setup.

Long-Core Displacement

The long-core displacement experiment aligns more closely with actual conditions, rendering the experimental results more representative. Figure 2 provides a schematic diagram of the long-core displacement system, which comprises an ISCO pump, storage vessels, a long-core holder, a back-pressure valve, and a flow meter, among other components. By assessing the oil and gas production from advanced injection and continuous injection, the recovery and CO_2 storage rates of various development methods were determined.

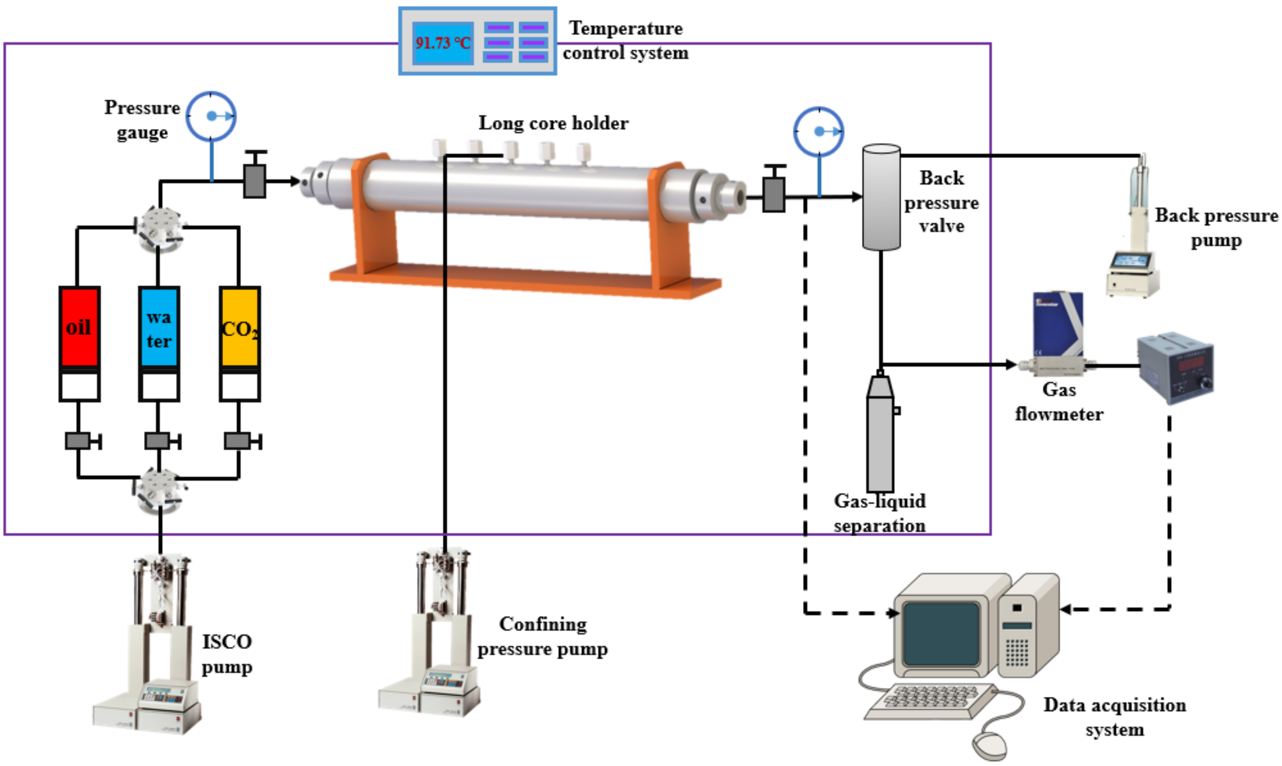

Figure 2. Schematic diagram of the long-core displacement experiment system.

2.1.3. Experimental Procedure

Slim Tube

Under reservoir temperature conditions, slim-tube experiments were conducted by establishing a series of experimental pressures and assessing the oil displacement efficiency at these various pressures. More dense testing was executed at the inflection point of the oil displacement efficiency. The specific experimental steps are as follows:

(1) Initially, the slim tube was saturated with kerosene. Subsequently, under reservoir conditions, reservoir live oil was injected to displace the kerosene within the slim tube, with the injection volume reaching 2 PV (double pore volumes). Continuous measurements of the volume and composition of the produced crude oil and gas at the outlet were undertaken until the composition of the outlet crude oil matched that of the live oil, signaling the conclusion of the saturation process;

(2) Displacement was carried out at a constant rate of 0.15 mL/min until there was no more oil production at the outlet, indicating the end of the displacement process;

(3) After adjusting the back-pressure value, changing the pressure, and cleaning the slim tube and experimental pipeline, steps (1) and (2) were repeated to determine the oil displacement efficiency under different pressures.

Long-Core Displacement

Core displacement experiments were conducted under reservoir temperature and pressure conditions. In order to make the experiment more representative, the specific experimental steps were as follows:

(1) After cutting and cleaning the core samples and drying them to remove any oil, they were subjected to a 24 h vacuum process. Afterwards, pressure was applied to saturate the core samples with formation brine;

(2) The core samples were arranged in a snug fit, and, to reduce the influence of the end effects, a piece of filter paper was placed between each core sample;

(3) The system was heated to a reservoir temperature of 91.73 °C and the back pressure was set to a reservoir pressure of 19.74 MPa in order to displace the formation with saturated crude oil until no more water flowed out of the core outlet. This process was carried out to achieve oil saturation;

(4) The displacement rate was set to 0.1 mL/min to conduct continuous gas displacement experiments, and the volumes of the produced fluids at different injection volumes were collected and recorded;

(5) To conduct the advanced CO_2 injection experiment, the core sample was replaced, and then steps (1)–(3) were repeated. We began by closing the outlet end of the core and injecting CO_2 until the system pressure stabilized and exceeded the original reservoir pressure by 4.0 MPa. Afterwards, CO_2 displacement at a rate of 0.1 mL/min was conducted, with the produced fluids at different injection volumes collected and recorded.

2.2. Simulation

2.2.1. Simulation Background

Advanced CO_2 injection. To enhance the performance of the gas injection development in the early stage, this study adopted the method of advanced CO_2 injection. Advanced CO_2 injection entails opening the injection well to introduce a substantial quantity of CO_2 into the reservoir and closing the production well prior to commencing production; essentially, it is engaging in injection without production. Following a period of gas injection, the production well is reopened, and conventional gas injection development is initiated. This method can effectively elevate the formation pressure, extend the stable production lives of production wells, and further enhance oil recovery. Concurrently, this method can also augment the interaction between the injected gas and crude oil, resulting in higher displacement efficiency.

Well pattern adjustment. For the phenomenon of severe gas channeling in the middle and late stages of gas injection development, this study proposes a method of well pattern adjustment to retard gas channeling and improve CO_2 storage: Adjust the square well pattern (initial well pattern) to the five-point well pattern or the row well pattern, as shown in Figure 3. Based on the constant injection volume in the block, the four horizontal production wells in the square well pattern are converted to gas injection wells, thereby realizing the transferring to a five-point well pattern.

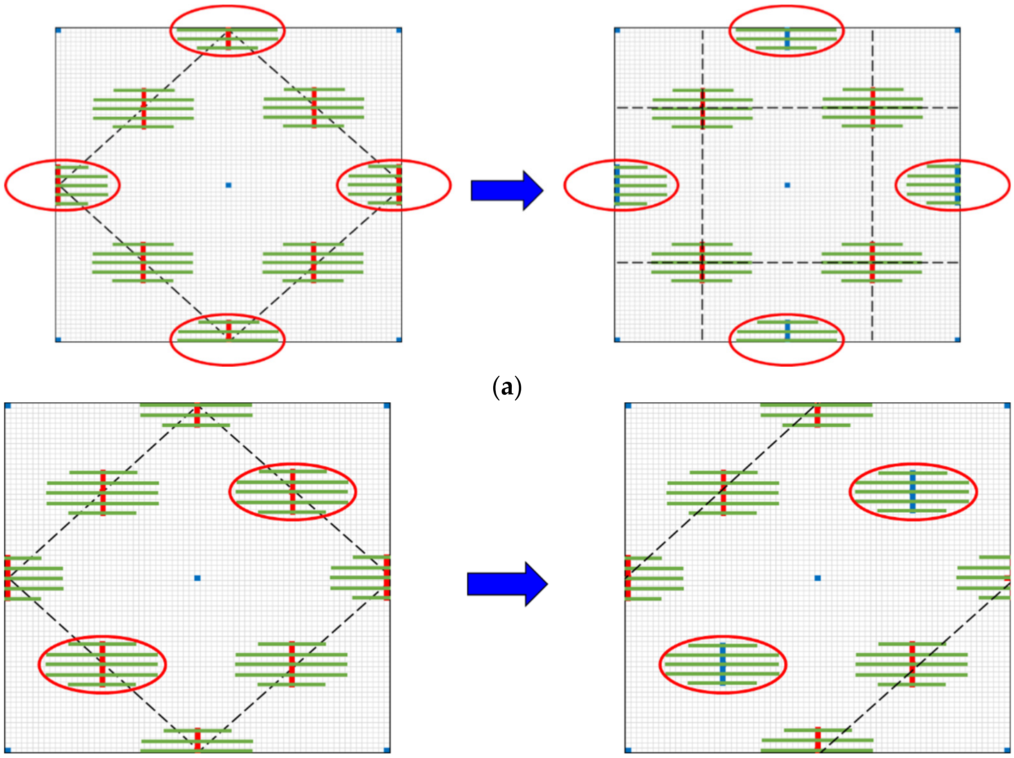

(**a**)

(**b**)

Figure 3. Well pattern adjustment method. (**a**) The transferring of a square well pattern to a five-point pattern. (**b**) The transferring of a square well pattern to a row well pattern.

The transferring of a square well pattern into a row well pattern is similar to the above-mentioned transformation, but the difference is that this method converts two side wells on the opposite sides of the square well pattern, thereby realizing the transferring to a row well pattern.

2.2.2. Numerical Simulation Model

The target reservoir for this study is the tight-oil reservoir in Block M of the Ordos Basin, with a buried depth of 2650 m, a formation thickness of 8.5 m, an average porosity of 8.1%, an average permeability of 0.28 mD, an initial oil saturation of 65%, and an original formation pressure of 19.74 MPa.

The phase change occurring during the dissolution and mass transfer process between the injected gas and formation fluid serves as the basis for accurately predicting the production performance of the gas injection development through the numerical simulation of multiphase and multicomponent systems, which can precisely characterize the phase behavior of the formation fluid. This study established a multiphase and multicomponent numerical model at reservoir scale based on geological characteristics and reservoir data, with the specific parameters delineated in Table 4. In alignment with the well pattern and well spacing utilized in Block M, a square well pattern with a well spacing of 425 m was employed for the injection and production wells. Development was facilitated through the use of a vertical well for injection and a horizontal well for production. Under the reservoir temperature 91.73 °C, the saturation pressure of the crude oil was 10.27 MPa. Based on the crude-oil composition data, the P–T phase diagram of all the components of the formation crude oil was calculated using the CMG-Winprop module (Figure 4), which is a coordinate graph that represents the changes in the system state parameters. It essentially serves as a graphical representation of the equation of state. The crude oil was divided into 10 pseudo-components through phase-state fitting (Table 5). Pseudo-components refer to the combination of components with similar properties as one component. The pseudo-component division results in a reduction in the number of components, which improves the speed of the numerical simulation and minimizes the impact on its accuracy. Figure 5 depicts the oil–water- and gas–liquid-phase relative permeability curves for the target reservoir. In the figure, Sw represents the water saturation, Sg signifies the gas saturation, and Krw, Krg, and Krl represent, respectively, the relative permeabilities of the water, gas, and liquid. Tables 4 and 5, along with Figures 4 and 5, provide a basis for the subsequent establishment of the numerical model.

Table 4. Basic parameters of numerical simulation model.

Model Parameter	Value
Number of grid blocks, x y z	69 × 69 × 1
Dimensions, x y z (m)	12.5 × 12.5 × 8.5
Length of horizontal well (m)	100
Horizontal-well spacing (m)	425
Long/short hydraulic-fracture half-length (m)	125/75
Hydraulic-fracture spacing (m)	25
Hydraulic-fracture conductivity (mD·m)	100
Matrix porosity (%)	8.1
Matrix permeability (mD)	0.28
Natural-fracture porosity (%)	0.5
Natural-fracture permeability (mD)	2.8
Natural-fracture spacing (m)	25
Initial oil saturation (%)	65
Reservoir temperature (°C)	91.73
Original formation pressure (MPa)	19.74

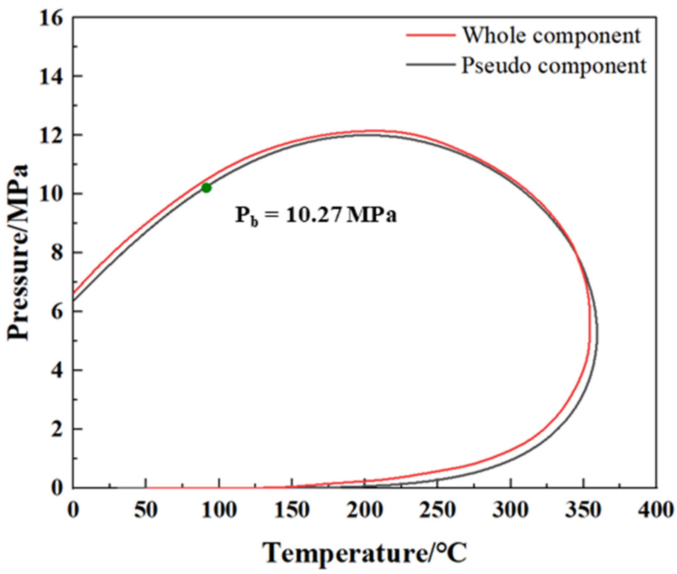

Figure 4. Well pattern adjustment method.

Table 5. Pseudo-component data of crude oil in tight reservoir.

Component	C_1	C_2	C_3	C_4	C_5	C_6-C_{13}	C_{14}-C_{19}	C_{20}-C_{30+}	CO_2	N_2
Content (%)	20.959	7.283	11.595	7.663	4.467	21.849	13.427	11.754	0.051	0.952

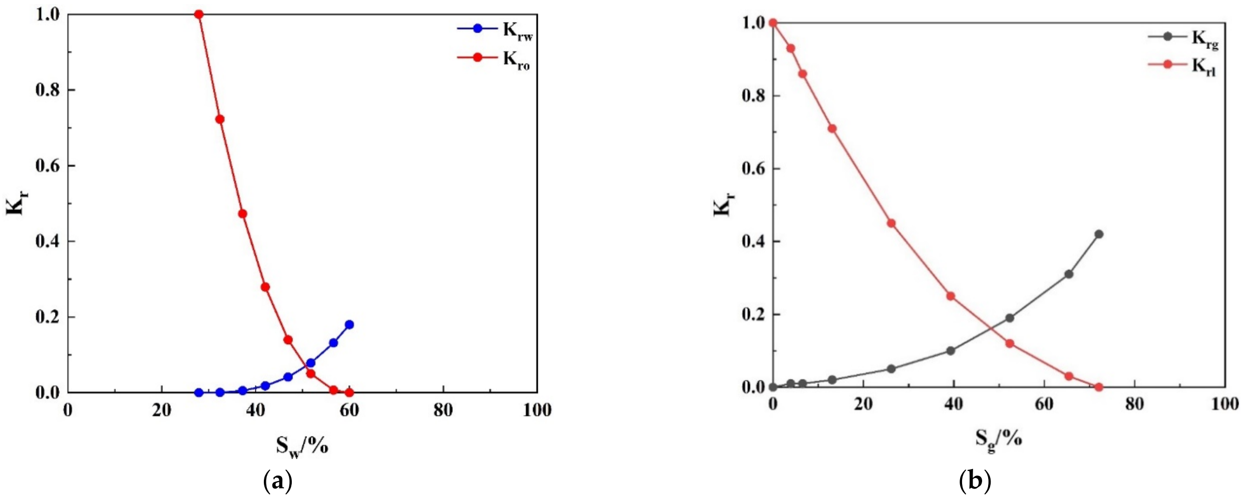

Figure 5. Relative permeability curves of tight-oil reservoir. (**a**) Oil–water relative permeability curve. (**b**) Gas–liquid relative permeability curve.

For the target tight reservoir, the effects of depletion or water injection development proved unsatisfactory, and gas channeling may have occurred during the gas injection development. Therefore, suitable development strategies need to be adopted to improve the development outcome and enhance oil recovery.

3. Results and Discussions

3.1. Experimental Results

3.1.1. MMP and Near-Miscibility Pressure Interval

Through slim-tube experiments, the oil displacement efficiency at varying injection pressures was obtained. The results of these experiments are illustrated in Figure 6. In traditional slim-tube experiments, classification is typically based on the non-miscible phase and the miscible phase. However, within the pressure range proximate to the MMP, the oil displacement efficiency does not escalate linearly; instead, it gradually deviates from a linear relationship and eventually transitions slowly into the miscible phase. Hence, a scenario termed the "near-miscibility pressure interval" arises [50]. The "near-miscibility pressure range" refers to a range of pressures that are close to but consistently lower than the MMP. Within this range, CO_2 and crude oil are not fully miscible but are in a transitional phase between non-miscible and miscible. The precise definition of "near-miscibility" currently lacks consensus both domestically and internationally [51]. However, a widely accepted method is to determine the miscibility state of the system based on the recovery. Specifically, a recovery exceeding 90% signifies that the CO_2 and crude oil have attained a miscible state. Conversely, when the recovery ranges between 80% and 90%, it is considered to be in the near-miscibility state, corresponding to the near-miscibility pressure range [52].

According to the method described, the near-miscibility pressure range for Block M was determined to be from 15.33 MPa to 18.47 MPa, with the MMP being 18.47 MPa, which allows for CO_2 miscible flooding. An analysis suggests that with increasing injection pressure, the oil displacement efficiency shows a linear increase. During this stage, the oil displacement primarily relies on the displacement action of CO_2, and this pressure range is categorized as non-miscible flooding. As the injection pressure continues to escalate, the CO_2 becomes more compatible with the crude oil, facilitating enhanced component exchange between them. CO_2 gradually exhibits its effects, including dissolution, expansion, and viscosity reduction. The relationship between the oil displacement efficiency and pressure diverges from a linear trend, achieving a higher level of oil displacement efficiency. Within this pressure range, the phenomenon is classified as near-miscible flooding. Subsequently, as the injection pressure further increases, the CO_2 and crude oil eventually reach a miscible state, and the oil displacement efficiency no longer significantly changes.

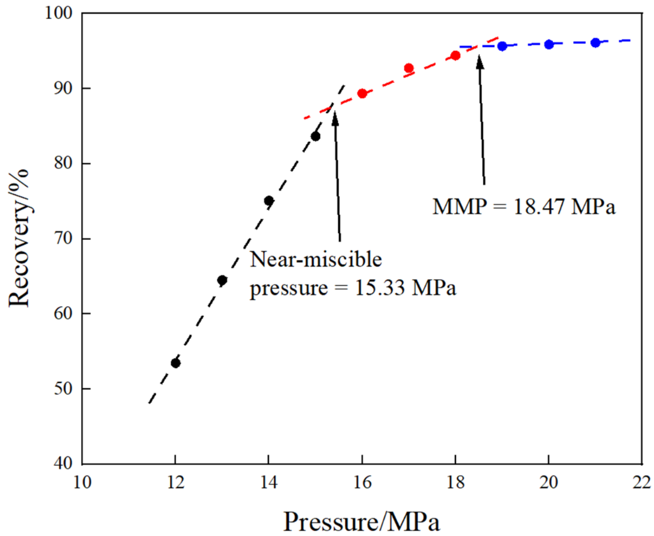

Figure 6. Results of slim-tube experiments.

3.1.2. Oil Recovery

Through the long-core displacement experiments, we obtained the gas displacement efficiency under two development scenarios: continuous CO_2 injection and advanced CO_2 injection. Figure 7 displays the curves of the oil recovery over time for continuous CO_2 injection and advanced CO_2 injection. The red and blue lines, respectively, depict the changes in the recovery for the advanced gas injection and continuous gas injection as a function of the amount of CO_2 injection. Under continuous CO_2 injection, the recovery was 66.82%, while under advanced CO_2 injection, the recovery was 71.65%. Compared to continuous CO_2 injection, advanced CO_2 injection increased the recovery by 4.83%.

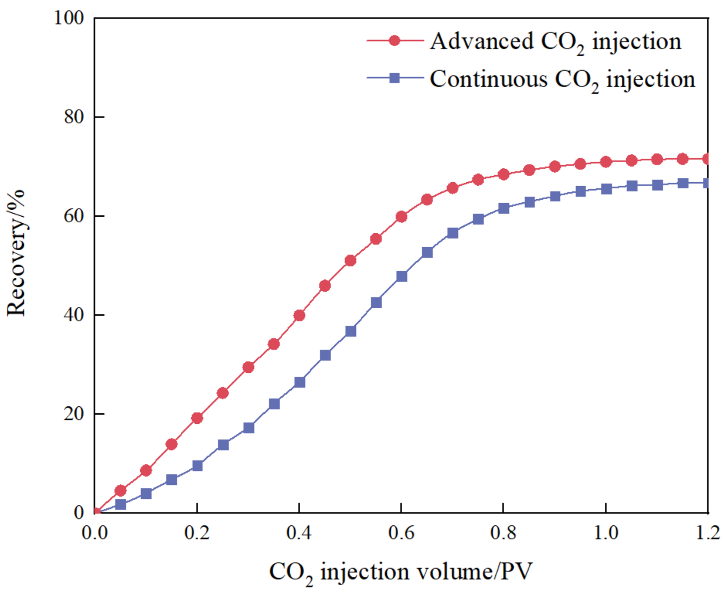

Figure 7. Relationship between recovery and CO_2 injection volume.

In the initial stages of continuous CO_2 injection, the primary mechanism for oil recovery hinges on CO_2 displacement. As some CO_2 dissolves in the crude oil, it is imperative to establish a sufficient displacement pressure difference, leading to a concave-down curve for the recovery with escalating CO_2 injection. With an increase in the CO_2 injection volume, the CO_2 begins to contribute to the expansion of the oil and the reduction in its viscosity, culminating in a sharp rise in the recovery. Upon the CO_2 injection volume reaching 0.65 PV, gas breakthrough transpires, and the oil recovery mechanism predominantly involves extraction and carrying actions. This shift results in an obvious reduction in the increase in the recovery, which eventually stabilizes. Advanced CO_2 injection involves injecting some CO_2 before the gas drive, increasing the reservoir pressure, and interacting with the crude oil, which reduces its viscosity. Therefore, the gas drive efficiency is higher, and the recovery shows a nearly linear increase with the injection volume. The increased reservoir pressure and reduced oil viscosity make the front edge of the advanced CO_2 injection more stable. When the injection volume reaches 0.7 PV, gas breakthrough occurs, and thereafter the recovery gradually increases until it stabilizes.

Figure 8 also illustrates the variation in the displacement pressure differences over time for continuous CO_2 injection and advanced CO_2 injection. The highest displacement pressure difference for continuous CO_2 injection is 5.2 MPa, while for advanced CO_2 injection, it is 6.65 MPa. Advanced CO_2 injection demonstrates a higher oil displacement efficiency, and, in the late stage of the gas drive, only a small amount of crude oil remains in the core pores, resulting in low gas flow resistance and a lower displacement pressure difference. These experimental results indicate that, under the same conditions, advanced CO_2 injection performs better in terms of the gas displacement efficiency compared to continuous CO_2 injection, and it also maintains a more stable displacement pressure difference.

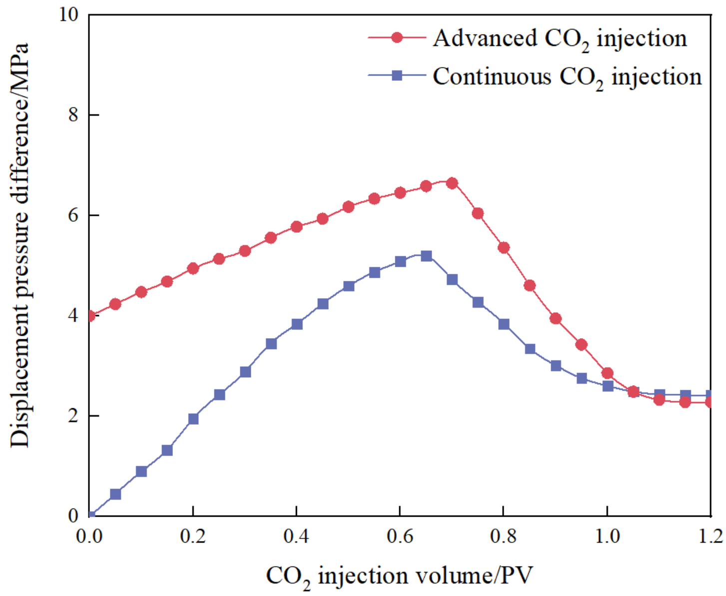

Figure 8. Relationship between displacement pressure difference and CO_2 injection volume.

3.1.3. CO_2 Storage

By evaluating the injection and production of CO_2, the CO_2 storage efficiency and volume for both continuous and advanced injection could be calculated. Figure 9 illustrates the variation in the CO_2 storage efficiency in correlation with the injection volume for both injection methodologies. In the initial stages of continuous injection, the CO_2 had not yet achieved breakthrough, and crude oil infused with CO_2 had not been produced, leading to a 100% CO_2 storage efficiency. As the injection volume escalated, dissolved CO_2 in the crude oil began to be produced, prompting a slight decrement in the CO_2 storage efficiency, which fell below 100%. Upon the occurrence of gas breakthrough, the CO_2 storage efficiency precipitously declined, ultimately registering at 38.22% for continuous injection. For advanced CO_2 injection, because the CO_2 was injected ahead of time and interacted with the crude oil, some CO_2 was already produced with the oil during the early gas displacement phase, leading to a CO_2 storage efficiency below 100%. When gas breakthrough occurred, the CO_2 storage efficiency rapidly decreased, reaching 40.51% in the end.

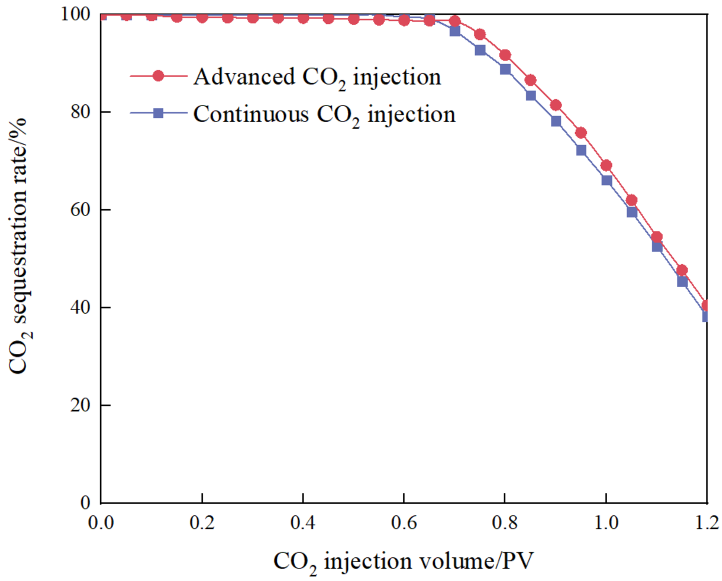

Figure 9. Relationship between CO_2 sequestration rate and CO_2 injection volume.

The primary mechanisms of CO_2 storage encompass structural storage, residual storage, dissolution storage, and mineralization storage [53,54]. Compared to continuous injection, advanced injection exhibits a higher oil displacement efficiency, as it dislodges more crude oil from the core, thereby availing more structural storage space for CO_2. However, advanced injection yields less residual oil, which is not conducive to CO_2 dissolution storage. Consequently, the CO_2 storage efficiency of advanced injection surpasses that of continuous injection, signifying that structural storage plays a more predominant role in the CO_2 storage efficiency, while the contribution of dissolution storage is relatively diminished.

3.2. Simulation Results

3.2.1. Optimization of Development Parameters

Injection Volume

In order to explore the influence of advanced CO_2 injection and the injection volume on the development effect, advanced-injection volumes of 0.02 PV, 0.03 PV, 0.04 PV, 0.05 PV, and 0.06 PV were designed via the experience of gas injection development and the actual situation in the Changqing Oilfield. Production prediction was simulated for 20 years to verify the development performance of advanced CO_2 injection and optimize the advanced-injection volume. Compared to conventional CO_2 injection development, advanced CO_2 injection can upraise the formation pressure by 12.21~32.88% and increase oil production by 2.16~10.50%, which proves that the effect of advanced CO_2 injection is better (Figure 10). Meanwhile, the CO_2 storage ratio improves with the increase in the advanced-injection volume. Especially in the early stage of gas injection development, the effects of the oil increase and CO_2 storage ratio are better.

The oil recovery increased with the increase in the advanced-injection volume, but when the injection volume exceeded 0.04 PV, the increase rate of the oil recovery became slower (Figure 11). During the 20-year development process, the oil recovery increased with the increase in the injection CO_2 volume, but the CO_2 storage ratio gradually decreased (Figure 12). Therefore, there was a collaborative optimization of the injection volume, which can enhance oil recovery and maximize the CO_2 storage ratio.

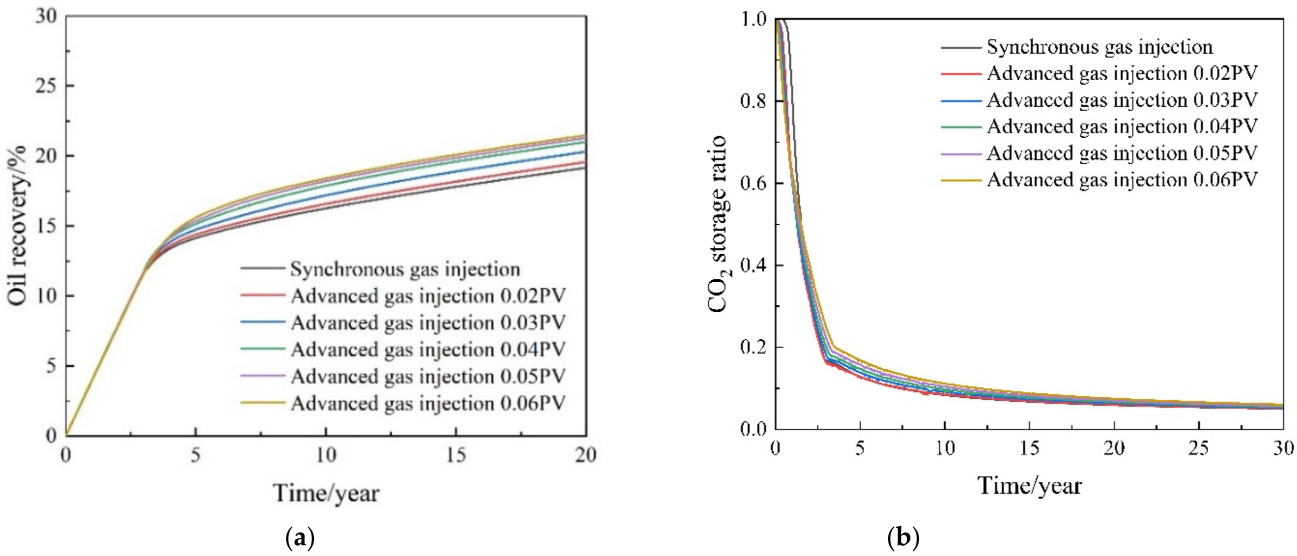

Figure 10. Oil recovery and CO_2 storage ratio at different advanced-injection volumes. (**a**) Oil recovery. (**b**) CO_2 storage ratio.

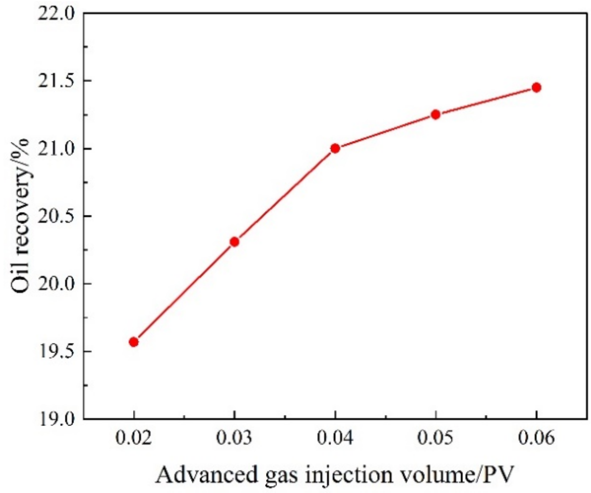

Figure 11. Relationship between injection volume and oil recovery.

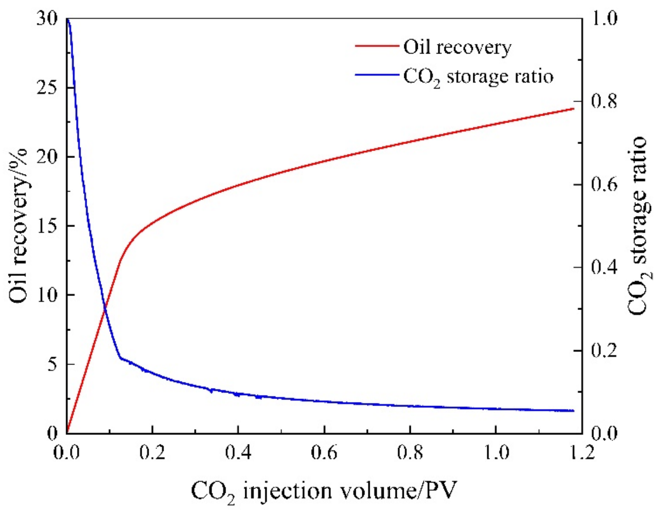

Figure 12. Relationship between oil recovery, CO_2 storage ratio, and injection volume.

In conjunction with the average formation pressure (Figure 13), it is observed that, at an injection volume of 0.04 PV, the degree of the formation pressure uplift is more favorable. Should the injection volume continue to increase, it would result in elevated injection costs and excessive production pressure differentials, which are adverse to oilfield production. Therefore, considering the optimal indicators, such as the oil recovery, CO_2 storage ratio, and average formation pressure, the reasonable advanced-injection volume is determined as 0.04 PV.

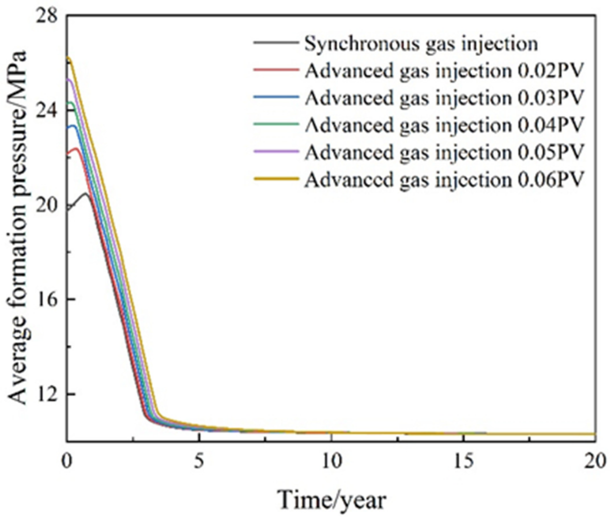

Figure 13. Average formation pressure at different advanced-injection volumes.

Bottom-Hole Pressure

In order to explore the impact of the bottom-hole pressure on the gas injection development, three different bottom-hole pressures of 8 MPa, 10 MPa, and 12 MPa were designed, and the production prediction was simulated for 20 years to optimize the bottom-hole pressure.

By comparing the oil recovery and CO_2 storage ratio of different bottom-hole pressures, the development effect was further analyzed. When the bottom-hole pressure is 8 MPa and 10 MPa, the oil recovery is higher, and a higher bottom-hole pressure can obtain a higher CO_2 storage ratio (Figure 14). However, when the formation pressure drops below the fluid saturation pressure (10.27 MPa), the formation crude oil will undergo degassing, increasing the density and viscosity of the crude oil, which is not conducive to subsequent gas injection development and adjustment. Simultaneously, at a bottom-hole pressure of 10 MPa, the gas–oil ratio does not escalate rapidly, the effect of gas channeling is minimized, and the sweep efficiency of the injected gas is higher (Figure 15). Therefore, taking into account both the oil recovery and CO_2 storage ratio comprehensively, a bottom-hole pressure of 10 MPa is recommended for the production well.

3.2.2. Well Pattern Adjustment

Transferring to Five-Point Well Pattern

For investigating the development performance of well pattern adjustment to the five-point method and the impact of the adjustment time on the development performance, five different adjustment times were designed: after 2 years, 3 years, 4 years, 5 years, and 6 years of gas injection development.

Upon transitioning to the five-point well pattern, both the oil recovery and CO_2 storage ratio improved (Figure 16), demonstrating the efficacy of this adjustment mode in gas injection development. Additionally, a notable reduction in the gas–oil ratio was observed (Figure 17), indicating that this adjustment mode effectively mitigates gas channeling.

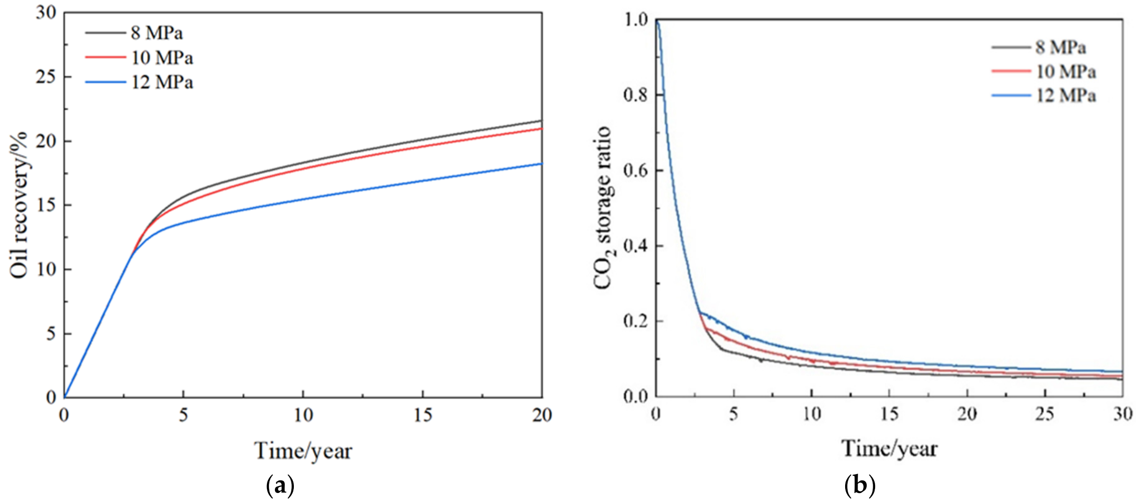

Figure 14. Oil recovery and CO_2 storage ratio at different bottom-hole pressures. (**a**) Oil recovery. (**b**) CO_2 storage ratio.

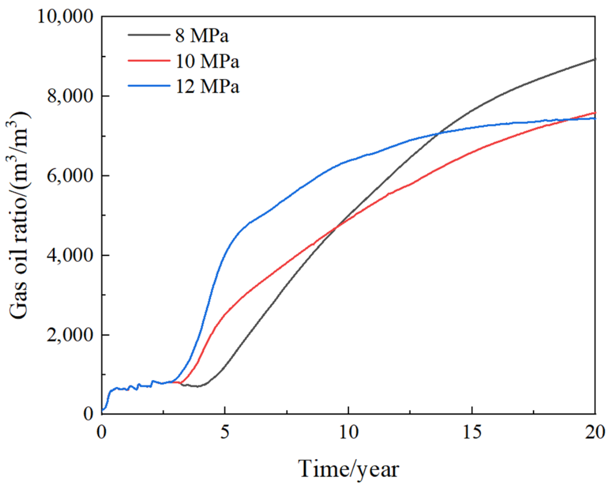

Figure 15. Gas–oil ratio at different bottom-hole pressures.

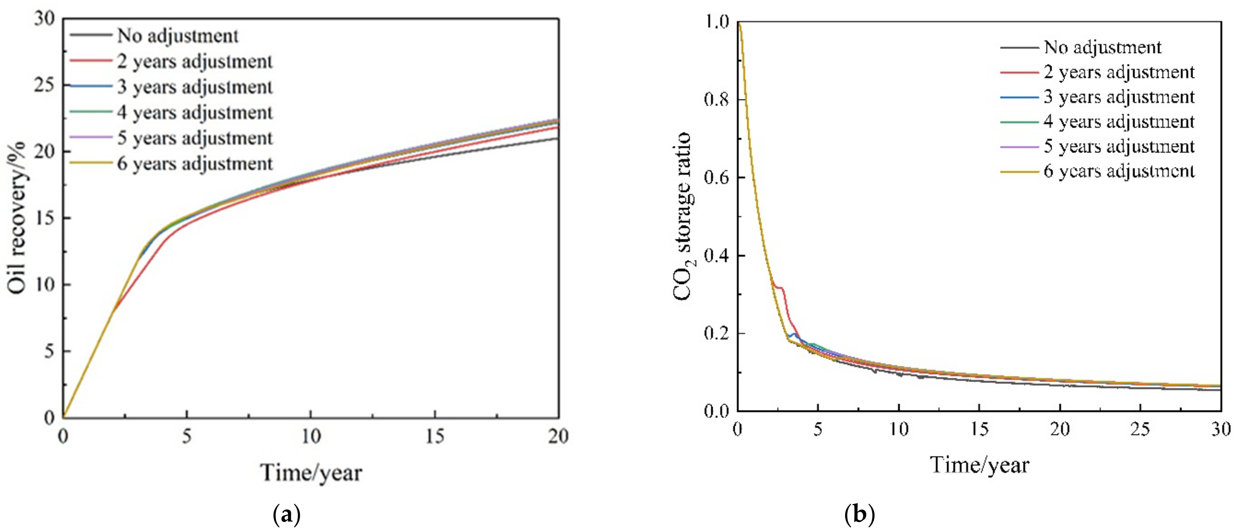

Figure 16. Oil recovery and CO_2 storage ratio after transferring to the five-point well pattern. (**a**) Oil recovery. (**b**) CO_2 storage ratio.

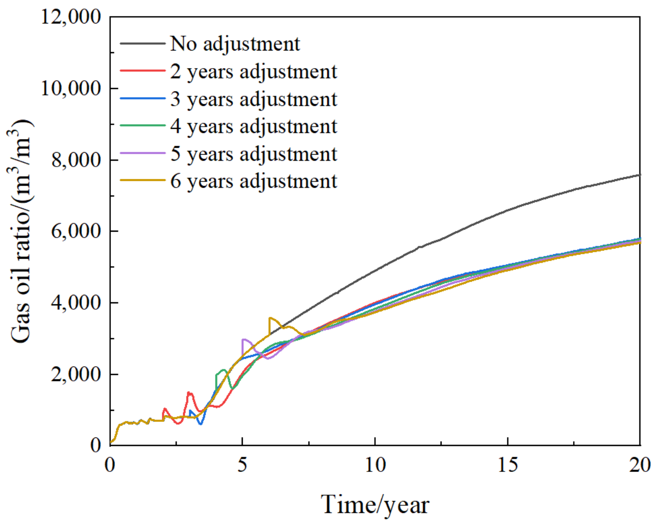

Figure 17. Gas–oil ratio after transferring to the five-point well pattern.

The adjustment of the well pattern effectively supplements the formation energy, elevates the average formation pressure (Figure 18), and effectively prolongs the stable production life while enhancing oil recovery. In conjunction with the distribution of the remaining oil after 20 years of gas injection development (Figure 19), the well pattern adjustment amplifies the sweep efficiency of the injected gas, thereby further exploiting the remaining oil.

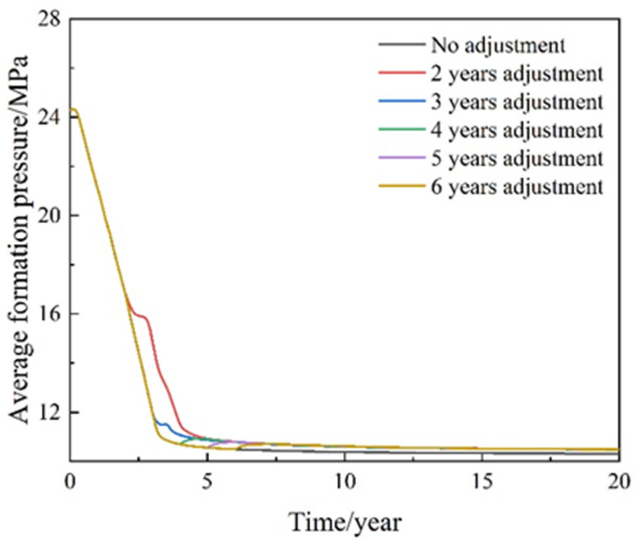

Figure 18. Average formation pressure after transferring to the five-point well pattern.

By comparing the oil recovery at the different times of well pattern adjustment (Figure 20), it can be seen that the highest oil recovery of 22.44% was achieved when the well pattern adjustment was conducted after 4 years of gas injection development. Other development indicators exhibited minor differences for varying adjustment times. Therefore, the optimal timing for transitioning from the square well pattern to the five-point well pattern is identified as 4 years after the gas injection development.

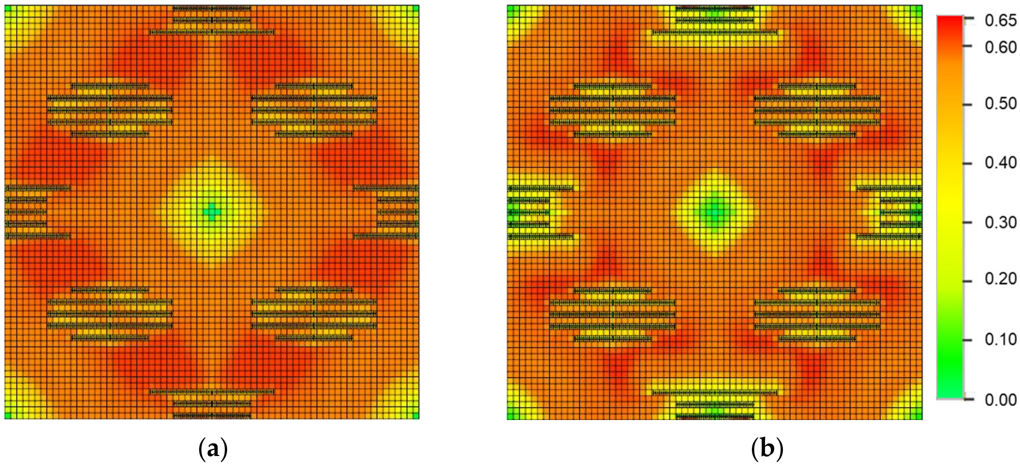

Figure 19. Oil saturation distribution after 20 years of development. (**a**) Square well pattern. (**b**) Transferring to the five-point well pattern.

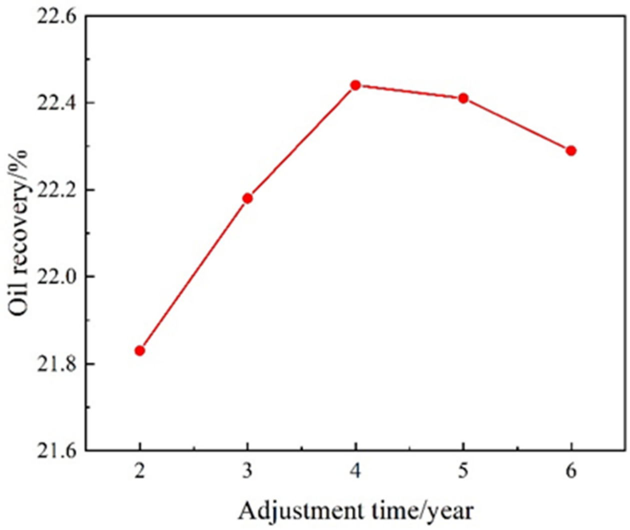

Figure 20. Relationship between oil recovery and adjustment time for square well pattern transferring to the five-point well pattern.

Transferring to Row Well Pattern

For studying the development regularity of the well pattern adjustment to the row method and the impact of the adjustment time on the development performance, five different adjustment times were designed: after 2 years, 3 years, 4 years, 5 years, and 6 years of gas injection development.

Similar to the five-point well pattern, the row well pattern significantly enhanced both the oil recovery and CO_2 storage ratio after 20 years of development (Figure 21), showcasing the positive impact of this adjustment mode on gas injection development. Concurrently, a notable reduction in the gas–oil ratio was observed (Figure 22), demonstrating that this adjustment mode can also effectively mitigate gas channeling.

This modification substantially augments the formation energy, enhances the mean formation pressure (as depicted in Figure 23), and effectively extends the duration of stable production, while also improving oil recovery. When combined with the distribution of the remaining oil after two decades of gas injection development (illustrated in Figure 24), the row well pattern elevates the sweep efficiency of the injected gas and further optimizes the extraction of the remaining oil.

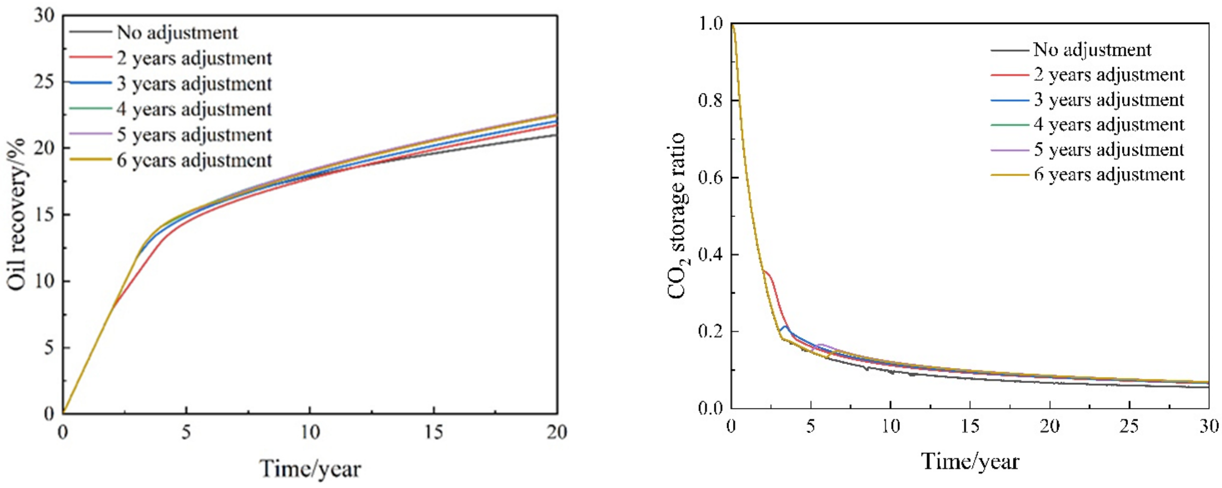

(a) (b)

Figure 21. Oil recovery and CO_2 storage ratio after transferring to the row well pattern. (**a**) Oil recovery. (**b**) CO_2 storage ratio.

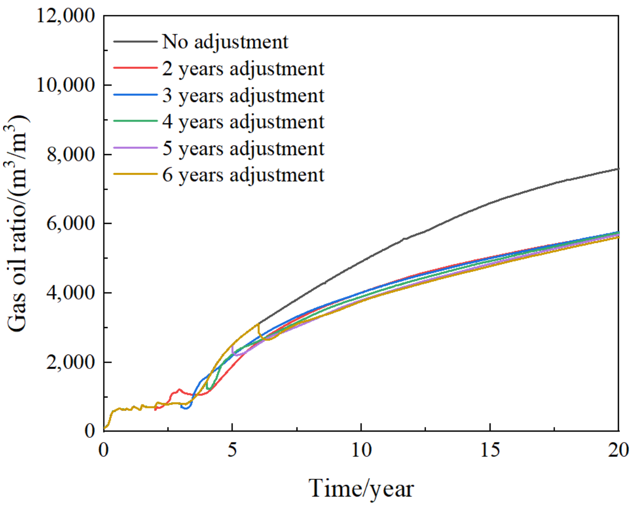

Figure 22. Gas–oil ratio after transferring to the row well pattern.

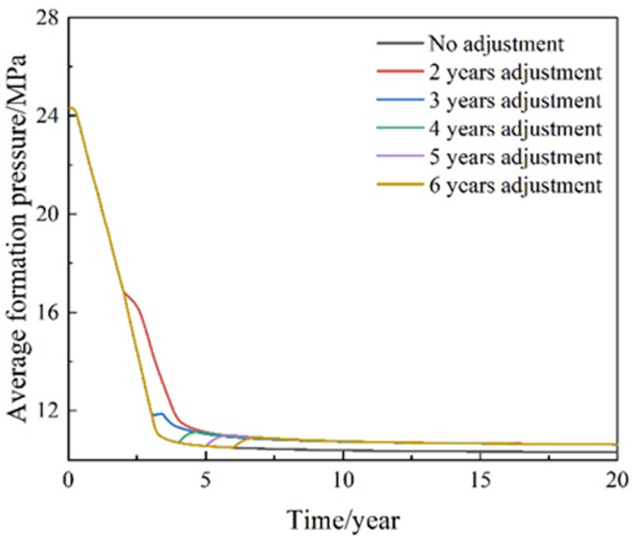

Figure 23. Average formation pressure after transferring to the row well pattern.

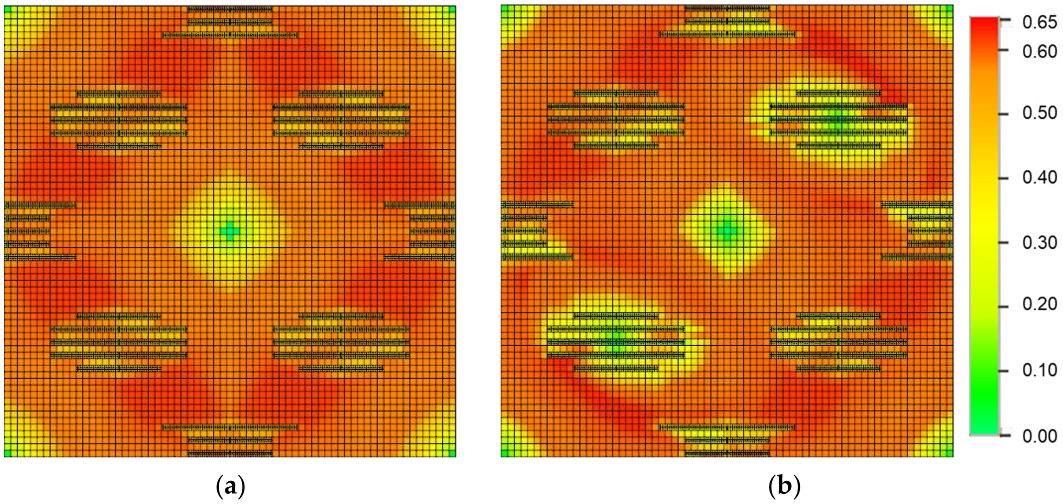

Figure 24. Oil saturation distribution after 20 years of development. (**a**) Square well pattern. (**b**) Transferring to the row well pattern.

Upon comparing the oil recovery at various time intervals of well pattern adjustment (as illustrated in Figure 25), it becomes evident that implementing the row well pattern after four years of gas injection development results in the highest recovery factor, which stands at 22.54%. There are only minor variations in the other development indicators for different adjustment timings. Therefore, the optimal time for transitioning from a square well pattern to a row well pattern is five years after the gas injection development.

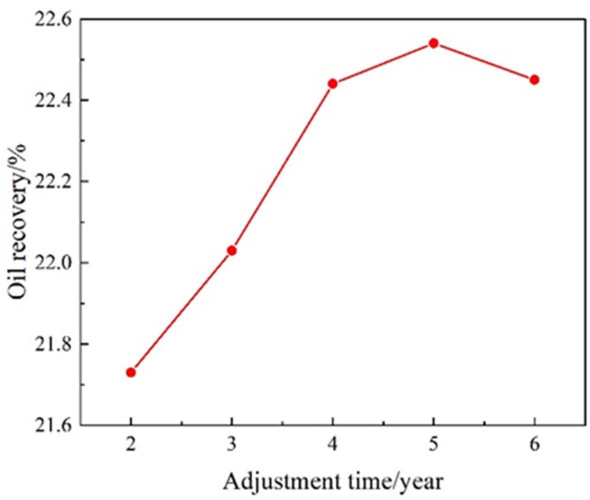

Figure 25. Relationship between oil recovery and adjustment time for square well pattern transferring to the row well pattern.

Comparison of Well Pattern Adjustments

Based on development indicators such as the oil recovery factor and formation pressure, a comparison was made between transferring to a five-point well pattern and transferring to a row well pattern, and the best pattern adjustment method was determined for tight reservoirs.

Both types of well pattern adjustments enhance the CO_2 storage and mitigate CO_2 channeling, as shown in Figure 26, with only minor differences between the two approaches. Nonetheless, the row well pattern outperforms the five-point well pattern in terms of the oil recovery and mean formation pressure, and it is more effective at enhancing the formation energy, as illustrated in Figure 27. Consequently, taking into account the optimal performance indicators, such as the oil recovery and mean formation pressure, the most appropriate pattern adjustment for Block M involves transitioning to the row well pattern.

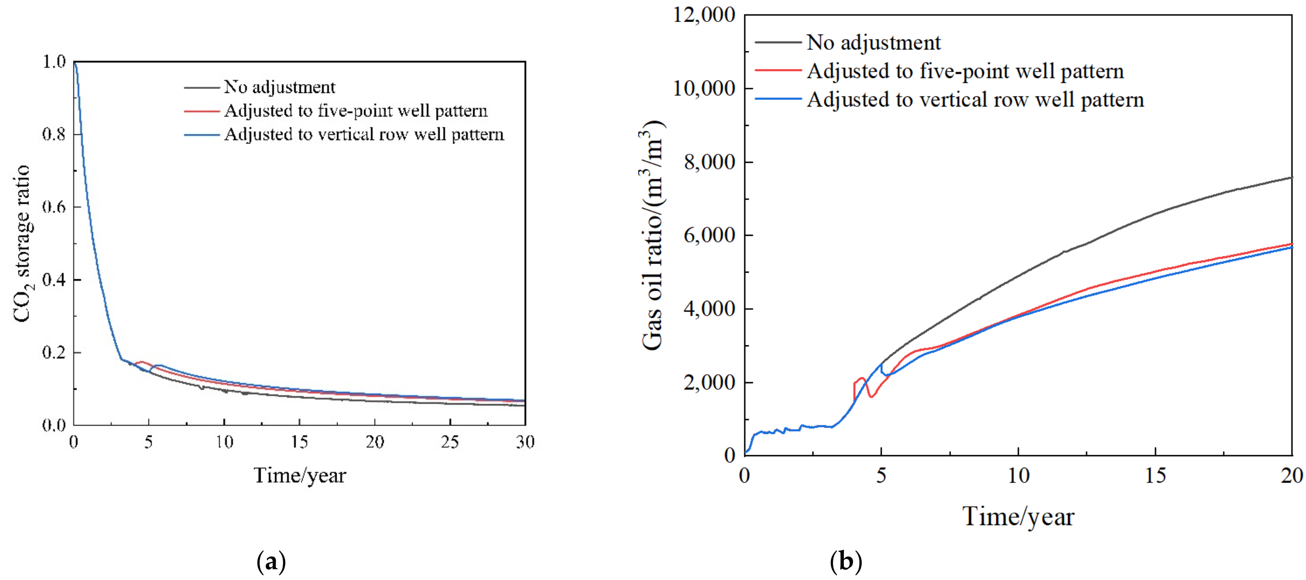

Figure 26. CO_2 storage ratio and gas–oil ratio after transferring well pattern. (**a**) CO_2 storage ratio. (**b**) Gas–oil ratio.

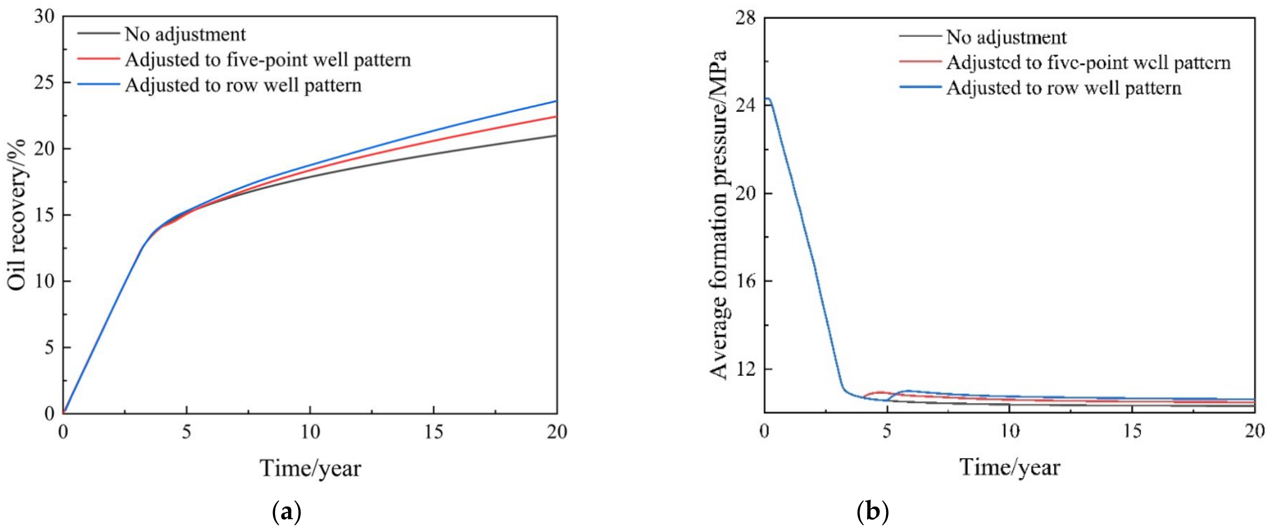

Figure 27. Development indicators after transferring well pattern. (**a**) Oil recovery. (**b**) Average formation pressure.

4. Conclusions

This paper employs the actual tight-oil reservoir in the Changqing Oilfield as a case study to innovatively examine the performance of advanced CO_2 injection techniques. It also establishes methods for well pattern adjustment aimed at improving CO_2 storage and enhancing oil recovery. This research offers theoretical guidance and serves as a reference for the development of tight reservoirs.

(1) The results of the slim-tube experiments indicate that the near-miscible pressure range in the study area is from 15.33 to 18.47 MPa, with an MMP of 18.47 MPa. Under reservoir pressure conditions, CO_2 miscible flooding can be achieved;

(2) The results of the long-core displacement experiments show that advanced CO_2 injection can effectively increase the recovery rate and achieve CO_2 sequestration. The recovery rate achieved via advanced CO_2 injection is 71.65%, which is 4.83% higher than

that observed with continuous CO_2 injection. Advanced CO_2 injection is more effective at facilitating CO_2 structural trapping; however, it also diminishes the volume of CO_2 that can be sequestered through dissolution. Moreover, the efficiency of advanced CO_2 injection is influenced by the total quantity of CO_2 injected. When compared to continuous CO_2 injection, the rate of CO_2 sequestration rises by 2.29%;

(3) Compared to conventional CO_2 injection development, advanced CO_2 injection can upraise the formation pressure by 12.21~32.88% and increase oil production by 2.16~10.50%. The optimal injection volume for advanced CO_2 injection was determined to be 0.04 PV, with the best bottom-hole flowing pressure of 10 MPa;

(4) Upon transitioning from a square well pattern to a five-point well pattern, the CO_2 storage ratio significantly improved, while the gas–oil ratio of the production wells correspondingly decreased. This adjustment in the well pattern effectively supplements the formation energy, prolongs the stable production phase of production wells, and enhances both the sweep efficiency and oil recovery;

(5) The impact of converting a square well pattern to a row well pattern shares similarities with that of transitioning from a five-point well pattern. This conversion effectively augments the CO_2 storage capacity and EOR. Nonetheless, the shift towards a row pattern is particularly advantageous in terms of reinforcing the formation energy. Consequently, in light of the prevailing conditions in tight reservoirs, it is advisable to consider the adjustment of the square well pattern in favor of the row well pattern.

Author Contributions: Methodology, T.S.; Software, J.Z.; Investigation, L.Z.; Resources, J.S.; Writing—original draft, X.H.; Visualization, H.T.; Supervision, H.Y. All authors have read and agreed to the published version of the manuscript.

Funding: This work was financially supported by the National Natural Science Foundation of China (52074317), Strategic Cooperation Technology Projects of CNPC and CUPB (ZLZX2020-02-04-04).

Data Availability Statement: Not applicable.

Conflicts of Interest: The authors declare no conflict of interest.

References

1. Yu, H.; Yang, Z.; Ma, T.; Lei, Z.; Cheng, S.; Chen, H. The feasibility of asynchronous injection alternating production for multistage fractured horizontal wells in a tight oil reservoir. *Pet. Sci. Bull.* **2018**, *3*, 32–44.
2. Guo, J.; Tao, L.; Zeng, F. Optimization of refracturing timing for horizontal wells in tight oil reservoirs: A case study of Cretaceous Qingshankou Formation, Songliao Basin, NE China. *Pet. Explor. Dev.* **2019**, *46*, 153–162. [CrossRef]
3. Yu, H.; Yang, Z.; Luo, L.; Liu, J.; Cheng, S.; Qu, X.; Lei, Q.; Lu, J. Application of cumulative-in-situ-injection-production technology to supplement hydrocarbon recovery among fractured tight oil reservoirs: A case study in Changqing Oilfield, China. *Fuel* **2019**, *242*, 804–818. [CrossRef]
4. Wang, Y.; Cheng, S.; Zhang, K.; He, Y.; Feng, N.; Qin, J.; Luo, L.; Yu, H. A Comprehensive Work Flow To Characterize Waterflood-Induced Fractures by Integrating Real-Time Monitoring, Formation Test, and Dynamic Production Analysis Applied to Changqing Oil Field, China. *SPE Reserv. Eval. Eng.* **2018**, *22*, 692–708. [CrossRef]
5. Qi, S.; Yu, H.; Xie, F.; Hu, M.; Lu, J.; Wang, Y. Experimental Investigation on the CO_2 Effective Distance and CO_2-EOR Storage for Tight Oil Reservoir. *Energy Fuels* **2022**, *37*, 339–349. [CrossRef]
6. Zhang, J.; Zhang, H.X.; Ma, L.Y.; Liu, Y.; Zhang, L. Performance evaluation and mechanism with different CO_2 flooding modes in tight oil reservoir with fractures. *J. Pet. Sci. Eng.* **2020**, *188*, 106950. [CrossRef]
7. Qin, G.; Dai, X.; Sui, L.; Geng, M.; Sun, L.; Zheng, Y.; Bai, Y. Study of massive water huff-n-puff technique in tight oil field and its field application. *J. Pet. Sci. Eng.* **2020**, *196*, 107514. [CrossRef]
8. Ma, N.; Li, C.; Wang, F.; Liu, Z.; Zhang, Y.; Jiang, L.; Shu, Y.; Du, D. Laboratory Study on the Oil Displacement Process in Low-Permeability Cores with Different Injection Fluids. *ACS Omega* **2022**, *7*, 8013–8022. [CrossRef]
9. Lashkarbolooki, M.; Ayatollahi, S. Experimental investigation on CO_2-light crude oil interfacial and swelling behavior. *Chin. J. Chem. Eng.* **2018**, *26*, 373–379. [CrossRef]
10. Tang, M.; Wang, C.; Deng, X.; Yang, H.; Lu, J.; Yu, H. Experimental investigation on plugging performance of nanospheres in low-permeability reservoir with bottom water. *Adv. Geo Energy Res.* **2022**, *6*, 95–103. [CrossRef]
11. Yu, H.; Wang, S.; Yang, H.; Yang, Y.; Zhang, J.; Wang, Y.; Yang, W.; Lu, J. A Systematic Method to Investigate the EOR Mechanism of Nanospheres: Laboratory Experiments from Core to Micro Perspective. *Energy Fuels* **2023**, *37*, 2053–2065. [CrossRef]
12. Qi, S.C.; Yu, H.-Y.; Han, X.-B.; Xu, H.; Liang, T.-B.; Jin, X.; Qu, X.-F.; Du, Y.-J.; Xu, K. Countercurrent imbibition in low-permeability porous media: Non-diffusive behavior and implications in tight oil recovery. *Pet. Sci.* **2023**, *20*, 322–336. [CrossRef]

13. Yu, H.; Chen, Z.; Lu, X.; Cheng, S.; Xie, Q.; Qu, X. Review of enhanced oil recovery by carbonated water injection. *Pet. Sci. Bull.* **2020**, *2*, 204–228.
14. Li, S.; Li, Z.; Dong, Q. Diffusion coefficients of supercritical CO_2 in oil-saturated cores under low permeability reservoir conditions. *J. CO_2 Util.* **2016**, *14*, 47–60. [CrossRef]
15. Li, H.; Zheng, S.; Yang, D. Enhanced swelling effect and viscosity reduction of solvent (s)/CO_2/heavy-oil systems. *SPE J.* **2013**, *18*, 695–707. [CrossRef]
16. Zhang, C.; Xi, L.; Wu, P.; Li, Z. A novel system for reducing CO_2-crude oil minimum miscibility pressure with CO_2-soluble surfactants. *Fuel* **2020**, *281*, 118690. [CrossRef]
17. Hemmati-Sarapardeh, A.; Ayatollahi, S.; Ghazanfari, M.H.; Masihi, M. Experimental determination of interfacial tension and miscibility of the CO_2–crude oil system; temperature, pressure, and composition effects. *J. Chem. Eng. Data* **2014**, *59*, 61–69. [CrossRef]
18. Abedini, A.; Mosavat, N.; Torabi, F. Determination of Minimum Miscibility Pressure of Crude Oil-CO_2 System by Oil Swelling/Extraction Test. *Energy Technol.* **2014**, *2*, 431–439. [CrossRef]
19. Cao, M.; Gu, Y. Oil recovery mechanisms and asphaltene precipitation phenomenon in immiscible and miscible CO_2 flooding processes. *Fuel* **2013**, *109*, 157–166. [CrossRef]
20. Xu, Z.X.; Li, S.Y.; Li, B.F.; Chen, D.Q.; Liu, Z.Y.; Li, Z.M. A review of development methods and EOR technologies for carbonate reservoirs. *Pet. Sci.* **2020**, *17*, 990–1013. [CrossRef]
21. Guo, Y.; Liu, F.; Qiu, J.; Xu, Z.; Bao, B. Microscopic transport and phase behaviors of CO_2 injection in heterogeneous formations using microfluidics. *Energy* **2022**, *256*, 124524. [CrossRef]
22. Hao, H.; Hou, J.; Zhao, F.; Song, Z.; Hou, L.; Wang, Z. Gas channeling control during CO 2 immiscible flooding in 3D radial flow model with complex fractures and heterogeneity. *J. Pet. Sci. Eng.* **2016**, *146*, 890–901. [CrossRef]
23. Zhao, F.; Wang, P.; Huang, S.; Hao, H.; Zhang, M.; Lu, G. Performance and applicable limits of multi-stage gas channeling control system for CO_2 flooding in ultra-low permeability reservoirs. *J. Pet. Sci. Eng.* **2020**, *192*, 107336. [CrossRef]
24. Zhang, Y.; Wang, Y.; Xue, F.; Wang, Y.; Ren, B.; Zhang, L.; Ren, S. CO_2 foam flooding for improved oil recovery: Reservoir simulation models and influencing factors. *J. Pet. Sci. Eng.* **2015**, *133*, 838–850. [CrossRef]
25. Liao, G.; He, D.; Wang, G.; Wang, L.; Wang, Z.; Su, C.; Qin, Q.; Bai, J.; Hu, Z.; Huang, Z.; et al. Discussion on the limit recovery factor of carbon dioxide flooding in a permanent sequestration scenario. *Pet. Explor. Dev.* **2022**, *49*, 1463–1470. [CrossRef]
26. Guofeng, W. Carbon dioxide capture, enhanced-oil recovery and storage technology and engineering practice in Jilin Oilfield, NE China. *Pet. Explor. Dev.* **2023**, *50*, 245–254.
27. Zhang, Y.; Di, Y.; Yu, W.; Sepehrnoori, K. A Comprehensive Model for Investigation of Carbon Dioxide Enhanced Oil Recovery with Nanopore Confinement in the Bakken Tight Oil Reservoir. *SPE Reserv. Eval. Eng.* **2018**, *22*, 122–136. [CrossRef]
28. Afari, S.; Ling, K.; Sennaoui, B.; Maxey, D.; Oguntade, T.; Porlles, J. Optimization of CO_2 huff-n-puff EOR in the Bakken Formation using numerical simulation and response surface methodology. *J. Pet. Sci. Eng.* **2022**, *215*, 110552. [CrossRef]
29. Yu, W.; Lashgari, H.R.; Sepehrnoori, K. Simulation study of CO_2 huff-n-puff process in Bakken tight oil reservoirs. In Proceedings of the SPE Western North American and Rocky Mountain Joint Meeting, Denver, CO, USA, 17–18 April 2014.
30. Sun, J.; Zou, A.; Sotelo, E.; Schechter, D. Numerical simulation of CO_2 huff-n-puff in complex fracture networks of unconventional liquid reservoirs. *J. Nat. Gas Sci. Eng.* **2016**, *31*, 481–492. [CrossRef]
31. Kamali, F.; Hussain, F.; Cinar, Y. A Laboratory and Numerical-Simulation Study of Co-Optimizing CO_2 Storage and CO_2 Enhanced Oil Recovery. *SPE J.* **2015**, *20*, 1227–1237. [CrossRef]
32. Sheng, J.J.; Chen, K. Evaluation of the EOR potential of gas and water injection in shale oil reservoirs. *J. Unconv. Oil Gas Resour.* **2014**, *5*, 1–9. [CrossRef]
33. Sun, L.; Dou, H.; Li, Z.; Hu, Y.; Hao, X. Assessment of CO_2 storage potential and carbon capture, utilization and storage prospect in China. *J. Energy Inst.* **2018**, *91*, 970–977. [CrossRef]
34. Shiyi, Y.; Qiang, W. New progress and prospect of oilfields development technologies in China. *Pet. Explor. Dev.* **2018**, *45*, 698–711.
35. Ren, B.; Duncan, I.J. Reservoir simulation of carbon storage associated with CO_2 EOR in residual oil zones, San Andres formation of West Texas, Permian Basin, USA. *Energy* **2018**, *167*, 391–401. [CrossRef]
36. Honarpour, M.M.; Nagarajan, N.R.; Grijalba, A.C.; Valle, M.; Adesoye, K. Rock-Fluid Characterization for Miscible CO_2 Injection: Residual Oil Zone, Seminole Field, Permian Basin. In Proceedings of the SPE Annual Technical Conference and Exhibition, Florence, Italy, 19–22 September 2010.
37. Jeschke, P.A.; Schoeling, L.; Hemmings, J. CO_2 flood potential of California oil reservoirs and possible CO_2 sources. In Proceedings of the SPE Annual Technical Conference and Exhibition, Dallas, TX, USA, 1–4 October 2000.
38. Luo, P.; Luo, W.; Li, S. Effectiveness of miscible and immiscible gas flooding in recovering tight oil from Bakken reservoirs in Sas-katchewan, Canada. *Fuel* **2017**, *208*, 626–636. [CrossRef]
39. Wang, X.; Luo, P.; Er, V.; Huang, S. Assessment of CO_2 flooding potential for Bakken formation, Saskatchewan. In Proceedings of the SPE Canada Unconventional Resources Conference, Calgary, AB, Canada, 19–21 October 2010.
40. Gong, Y.; Gu, Y. Miscible CO_2 simultaneous water-and-gas (CO2-SWAG) injection in the Bakken formation. In Proceedings of the SPE/CSUR Unconventional Resources Conference, Calgary, AB, Canada, 20–22 October 2015.
41. Li, Q.; Han, Y.; Liu, X.; Ansari, U.; Cheng, Y.; Yan, C. Hydrate as a by-product in CO_2 leakage during the long-term sub-seabed sequestration and its role in preventing further leakage. *Environ. Sci. Pollut. Res.* **2022**, *29*, 77737–77754. [CrossRef] [PubMed]

42. Li, Q.; Wang, F.; Wang, Y.; Forson, K.; Cao, L.; Zhang, C.; Zhou, C.; Zhao, B.; Chen, J. Experimental investigation on the high-pressure sand suspension and adsorption capacity of guar gum fracturing fluid in low-permeability shale reservoirs: Factor analysis and mechanism disclosure. *Environ. Sci. Pollut. Res.* **2022**, *29*, 53050–53062. [CrossRef] [PubMed]
43. Yi, L.; Shenglai, Y.; Xing, Z. Experimental research on CO_2 miscible flooding by advanced gas injection in low permeability reservoir. *Pet. Geol. Recovery Effic.* **2012**, *19*, 78–80.
44. Wang, J.-F.; Jiang, T.-W.; Chen, Q.; Chen, J.; Ma, X.-L.; Gai, C.-C. Research on Synergistic Development Technology of Advanced Gas Injection and Oil Accumulation Jointed Under Gas-Oil-Geothermal Storage Based on Molecular Sieve and Component Gradient Effect. In Proceedings of the International Field Exploration and Development Conference, Xi'an, China, 16–18 November 2022; Springer Nature: Singapore, 2022; pp. 4338–4351.
45. Liu, Y.; Rui, Z. A Storage-Driven CO_2 EOR for a Net-Zero Emission Target. *Engineering* **2022**, *18*, 79–87. [CrossRef]
46. Zhang, X.; Wei, B.; Shang, J.; Gao, K.; Pu, W.; Xu, X.; Wood, C.; Sun, L. Alterations of geochemical properties of a tight sandstone reservoir caused by supercritical CO2-brine-rock interactions in CO_2-EOR and geosequestration. *J. CO_2 Util.* **2018**, *28*, 408–418. [CrossRef]
47. Liu, Y.; Rui, Z.; Yang, T.; Dindoruk, B. Using propanol as an additive to CO_2 for improving CO_2 utilization and storage in oil reservoirs. *Appl. Energy* **2022**, *311*, 118640. [CrossRef]
48. Ren, B.; Jeong, H. Influence of injection strategies on local capillary trapping during geological carbon sequestration in saline aquifers. *J. CO_2 Util.* **2018**, *27*, 441–449. [CrossRef]
49. Syed, F.I.; Muther, T.; Van, V.P.; Dahaghi, A.K.; Negahban, S. Numerical trend analysis for factors affecting EOR performance and CO_2 storage in tight oil reservoirs. *Fuel* **2022**, *316*, 123370. [CrossRef]
50. Yu, H.; Lu, X.; Fu, W.; Wang, Y.; Xu, H.; Xie, Q.; Qu, X.; Lu, J. Determination of minimum near miscible pressure region during CO_2 and associated gas injection for tight oil reservoir in Ordos Basin, China. *Fuel* **2019**, *263*, 116737. [CrossRef]
51. Chen, H.; Liu, X.L.; Jia, N.H.; Zhang, K.; Yang, R.; Yang, S. Prospects and key scientific issues of CO_2 near-miscible flooding. *Pet. Sci. Bull.* **2020**, *5*, 392–401.
52. Chen, H.; Li, B.; Zhang, X.; Wang, Q.; Wang, X.; Yang, S. Effect of gas contamination and well depth on pressure interval of CO_2 near-miscible flooding. *J. Pet. Sci. Eng.* **2019**, *176*, 43–50. [CrossRef]
53. Bachu, S.; Bonijoly, D.; Bradshaw, J.; Burruss, R.; Holloway, S.; Christensen, N.P.; Mathiassen, O.M. CO_2 storage capacity estimation: Methodology and gaps. *Int. J. Greenh. Gas Control* **2007**, *1*, 430–443. [CrossRef]
54. Ji, M.; Kwon, S.; Choi, S.; Kim, M.; Choi, B.; Min, B. Numerical investigation of CO_2-carbonated water-alternating-gas on enhanced oil recovery and geological carbon storage. *J. CO_2 Util.* **2023**, *74*, 102544. [CrossRef]